Supporting Information

A Synergy between Push-Pull Electronic Effect and Twisted Conformation for High-Contrast Mechanochromic AIEgens

Xiaoxuan Wang,[a, #] Chunxuan Qi,[a, #] Zhiyuan Fu,[c] Haoke Zhang,[b] Jianguo Wang,[d] Hai-Tao Feng, *[a] Kai Wang,[c] Bo Zou, *[c] Jacky W. Y. Lam[b] and Ben Zhong Tang*[b]

[a]AIE Research Center, Shaanxi Key Laboratory of Phytochemistry, College of Chemistry and Chemical Engineering, Baoji University of Arts and Sciences, Baoji 721013, China

[b]Department of Chemistry, Hong Kong Branch of Chinese National Engineering Research Center for Tissue Restoration & Reconstruction, Institute for Advanced Study, Department of Chemical and Biomedical Engineering, Division of Life Science, State Key Laboratory of Molecular Neuroscience, The Hong Kong University of Science and Technology, Clear Water Bay, Hong Kong, China

[c]State Key Laboratory of Superhard Materials, Jilin University, Changchun 130012, P. R. China

[d]College of Chemistry and Chemical Engineering, Inner Mongolia Key Laboratory of Fine Organic Synthesis, Inner Mongolia University, Hohhot 010021, P. R. China.

Corresponding authors: Hai-Tao Feng (haitaofeng907@163.com), Bo Zou (zoubo@jlu.edu.cn), Ben Zhong Tang (tangbenz@ust.hk)

Table of Contents

1. General information

Materials: All reagents and solvents were chemical pure (CP) grade or analytical reagent (AR) grade and were used as received unless otherwise indicated.

Measurements: ^{1}H NMR and ^{13}C NMR spectra were measured on a Bruker AV 400 spectrometer at 298 K in $CDCl_3$. Infrared spectra were recorded on BRUKER EQUINAX55 spectrometer. Absorption spectra were recorded on a Hewlett-Packard 8453 UV-vis spectrophotometer. High-resolution mass spectra (HRMS) were obtained on a GCT Premier CAB 048 mass spectrometer operated in MALDI-TOF mode. Photoluminescence spectra were collected on a Shimadzu RF-5301 fluorophotometer at 298 K. Solid-state quantum yield was measured using a Hamamatsu C11347 Quantaurus-QY integrating sphere. The lifetime was measured on a Edinburgh FLS980 fluorescence spectrophotometer equipped with a continuous xenon lamp (Xe1). A picosecond pulsed diode laser (EPL-375) was used as the light source. The impulse response function (IRF) was from the output of pulsed diode laser. The data were analyzed using FAST software through a double-exponential model for lifetime. The fit algorithm ensures fast and robust convergence with a maximum of independence of the start parameters. A shift between the measured sample kinetics and the IRF as well as a constant background of both the IRF and the sample decay can be computed automatically or can be fixed to predefined values. All lifetimes have been fitted to the raw data by means of reconvolution fits (fits that use both the double-exponential function and the IRF to calculate the theoretical fluorescence decay curve). The lifetime data were collected at fixed emission wavelengths (their maximum emission wavelength). The average fluorescence lifetime calculated by $\tau_{av} = \sum A_i\tau_i^2/\sum A_i\tau_i$, where A_i represent the fractional weights of the various decay time components τ_i of the multi-exponential fitting. χ^2 is the uncertainty values of lifetimes.

Single crystal data were collected on a Bruker Smart APEXII CCD diffractometer using graphite monochromated Mo Kα radiation (λ = 0.71073 Å) or Cu Kα radiation (λ = 1.54184 Å). A symmetric DAC with 400 μm diameter culet diamonds was used in high-pressure fluorescence, absorption and synchrotron Raman experiments. A T301 steel gasket with a 130 μm diameter hole in the center was placed between the parallel diamonds. The gasket with hole was used as the sample-containing compartment. Crystals were loaded in the gasket hole together with a small ruby ball to measure the pressure by using the standard ruby-fluorescence method. Silicone oil was used as the pressure-transmitting medium. The pressure conditions were ensured by monitoring the separation and width of ruby R1 and R2 lines. All of the high-pressure experiments were conducted at room temperature. In situ fluorescent measurements under high pressure were performed on an Ocean Optics QE65000 spectrometer in the reflection mode. In situ high-pressure absorption spectra were recorded by an optical fiber spectrometer (Ocean Optics, QE65000). The real optical photographs were obtained by using a Nikon Ti-U microscope equipped with a digital colour camera. High-pressure Raman spectra were recorded using Horiba iHR550 spectrograph.

Computational calculations

All the calculations were performed by Gaussian 09 software using density functional theory at B3LYP/6-311G** level.

2. Synthesis

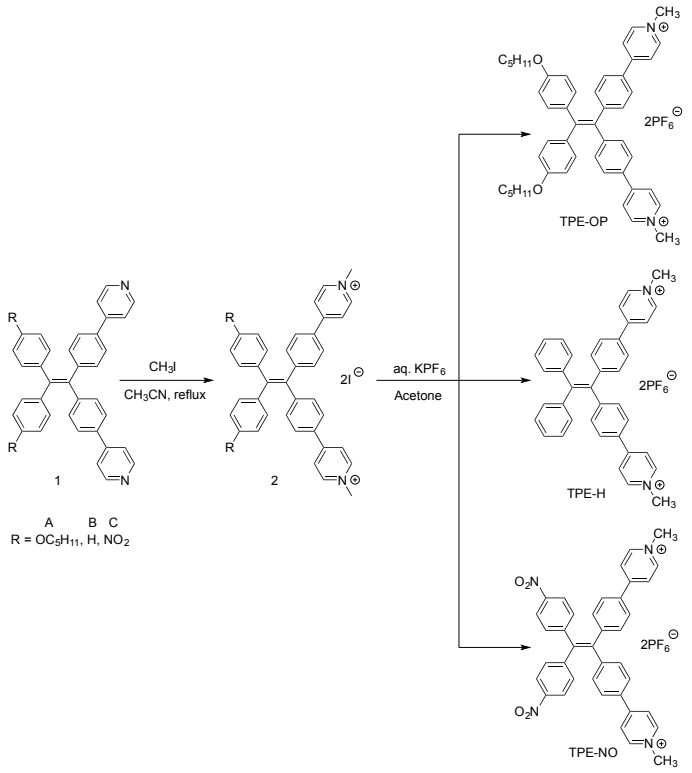

Scheme S1. Synthetic procedure of TPE-OP, TPE-H and TPE-NO.

Compound **1A-1C** are known molecules and were synthesized according to the previous publications.[1,2] Their characterization data are given below.

Compound **1A**: ^{1}H NMR (400 MHz, $CDCl_3$) δ = 0.85 (t, J = 7.0 Hz, 6 H), 1.32 (m, 8 H), 1.64 (m, 4 H), 3.86 (t, J = 8.8 Hz, 4 H), 6.70 (d, J = 8.7 Hz, 4 H), 6.90 (d, J = 8.7 Hz, 4 H), 7.10 (d, J = 8.4 Hz, 4 H), 7.64 (d, J = 8.4 Hz, 4 H), 7.66 (d, J = 6.1 Hz, 4 H), 8.57 (d, J = 6.1 Hz, 4 H). ^{13}C NMR ($CDCl_3$, 100 MHz) δ = 158.1, 149.6, 148.3, 145.5, 142.3, 137.0, 135.5, 135.1, 132.6, 132.2, 126.3, 121.3, 113.7, 67.8, 28.9, 28.2, 22.4, 14.0. IR (KBr) v = 3070, 3030, 2930, 2860, 1597, 1506, 1466, 1397, 1243, 1175, 1052, 989, 805 cm^{-1}. ESI^{+} HRMS m/z calcd for $C_{46}H_{47}N_2O_2$ 660.3671 [M+H], found 660.3685 [M+H].

Compound **1B**: ^{1}H NMR (300 MHz, CD_2Cl_2) δ = 8.60 (d, J = 6.3 Hz, 4 H), 7.47–7.52 (m, 8

H), 7.14–7.23 (m, 10 H), 7.08–7.12 (m, 4 H). The ^{13}C NMR (CD_2Cl_2, 75 MHz) δ = 121.35, 126.44, 127.00, 128.05, 131.39, 132.24, 136.17, 143.59, 144.74, 147.51, 150.49. ESI^+ HRMS m/z calcd for $C_{36}H_{27}N_2$, 487.2174 [M+H], found 487.2176 [M+H].

Compound **1C**: ^1H NMR (400 MHz, $CDCl_3$) δ = 7.16 (d, J = 8.3 Hz, 4 H), 7.22 (d, J = 8.8 Hz, 4 H), 7.50 (d, J = 8.0 Hz, 4 H), 7.53 (d, J = 5.7 Hz, 4 H), 8.04 (d, J = 8.8 Hz, 4 H), 8.66 (d, J = 6.0 Hz, 4 H) ppm. ^{13}C NMR (100 MHz, $CDCl_3$) δ = 149.5, 148.9, 147.8, 146.7, 144.6, 142.5, 138.1, 137.4, 132.0, 131.9, 127.0, 123.6, 121.5 ppm. IR (KBr) ν = 3099, 3070, 3028, 2925, 2846, 1593, 1513, 1488, 1400, 1343, 1107, 1012, 816,707 cm^{-1}. ESI^+ HRMS m/z calcd for $C_{36}H_{25}N_4O_4$ 577.1876 [M+H], found 577.1854 [M+H].

Compound TPE-OP, TPE-H and TPE-NO were synthesized according to our previous publication.[3] Their synthetic procedure and characterization data are given below.

Synthesis of TPE-OP: To a one-neck 50 mL flask, iodomethane (0.85 mL, 13.65 mmol) and compound **1A** (0.3 g, 0.455 mmol) were dissolved in CH_3CN (10 mL) and then refluxed for 1 h. After reaction completion monitored by TLC, the solvent (CH_3CN) was removed under vacuum. The obtained solid without further purification was dissolved in acetone (10 mL). Then a saturated aqueous solution of KPF_6 (2 mL) was added in this system. After stirring for 1 h at room temperature, the solvent was removed under vacuum and the crude product was purified by recrystallization to give an orange powder in 63% yield. ^1H NMR (400 MHz, MeOD) δ = 0.92 (t, J = 6.8 Hz, 6 H), 5.59 (m, 8 H), 1.72 (m, 4 H), 6.00 (t, J = 6.4 Hz, 4 H), 4.34 (s, 6 H), 6.67 (d, J = 8.8 Hz, 4 H), 6.96 (d, J = 8.8 Hz, 4 H), 7.27 (d, J = 8.4 Hz, 4 H), 7.80 (d, J = 8.4 Hz, 4 H), 8.28 (d, J = 6.8 Hz, 4 H), 8.76 (d, J = 6.8 Hz, 4 H) ppm. ^{13}C NMR (100 MHz, DMSO-d_6) δ = 157.6, 153.1, 147.4, 145.2, 135.9, 134.5, 132.0, 131.9, 130.8, 127.5, 123.3, 113.7 ppm. ^{31}P NMR (160 MHz, DMSO-d_6) δ = -144.3 ppm. ESI^+ HRMS m/z calcd for $C_{48}H_{53}F_6N_2O_2P^+$ 834.3743, found 834.3702.

Synthesis of TPE-H: The procedure was similar to that of TPE-OM. TPE-H prepared from **1B** was obtained as a yellow solid (yield, 69%). ^1H NMR (400 MHz, Acetone-d_6) δ = 4.60 (s, 6 H), 7.17 (m, 4 H), 7.22 (m, 6 H), 7.39 (d, J = 8.4 Hz, 4 H), 7.96 (d, J = 8.4 Hz, 4 H), 8.51 (d, J = 6.8 Hz, 4 H), 9.05 (d, J = 6.8 Hz, 4 H) ppm. ^{13}C NMR (100 MHz, Acetone-d_6) δ =

154.3, 146.8, 144.9, 144.0, 142.1, 137.8, 131.9, 131.3, 130.3, 127.3, 127.0, 126.7 123.6 ppm. ^{31}P NMR (160 MHz, DMSO-d_6) δ = -144.4 ppm. ESI$^+$ HRMS m/z calcd for $C_{38}H_{32}F_6N_2P^+$ 661.2202, found 661.2212.

Synthesis of TPE-NO: The procedure was similar to that of TPE-OM. TPE-NO_2 prepared from **1C** was obtained as a yellow solid (yield, 69%). ^{1}H NMR (400 MHz, Acetone-d_6) δ = 4.61 (s, 6 H), 7.49 (d, J = 8.4 Hz, 8 H), 8.02 (d, J = 8.4 Hz, 4 H), 8.12 (d, J = 8.8 Hz, 4 H), 8.52 (d, J = 6.8 Hz, 4 H), 8.51 (d, J = 6.8 Hz, 4 H) ppm. ^{13}C NMR (100 MHz, Acetone-d_6) δ = 154.1, 148.0, 146.2, 145.0, 144.9, 139.5, 132.5, 131.7, 131.6, 127.3, 123.9, 122.7 ppm. ^{31}P NMR (160 MHz, DMSO-d_6) δ = -144.4 ppm. ESI$^+$ HRMS m/z calcd for $C_{38}H_{30}F_6N_4O_4P^+$ 751.1903, found 751.1897.

3. Photophysical properties of TPE-OP, TPE-H and TPE-NO.

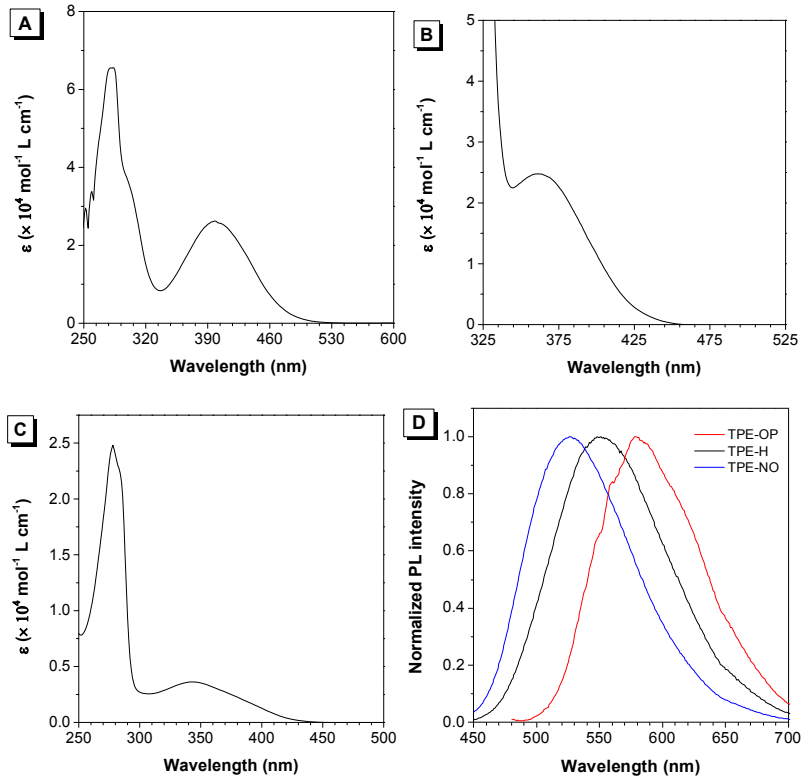

Figure S1. UV-vis spectra of TPE-OP (A), TPE-H (B), TPE-NO (C) in THF solution, [TPE-OP] = [TPE-H] = [TPE-NO] =1.0 × 10^{-5} M and their PL spectra (D) in the aggregate state, λ_{ex} = 390 nm.

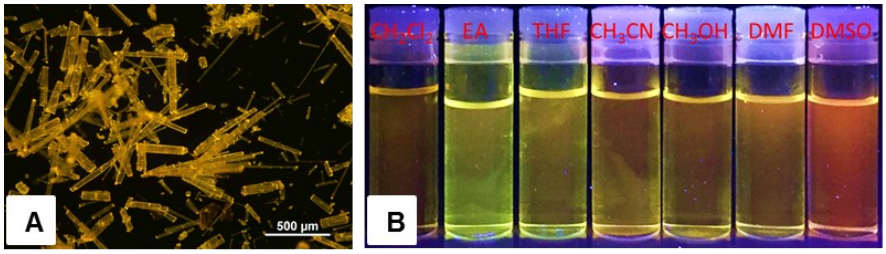

Figure S2. Fluorescent images of TPE-OP in crystals and different solvents taken under 365 nm UV irradiation.

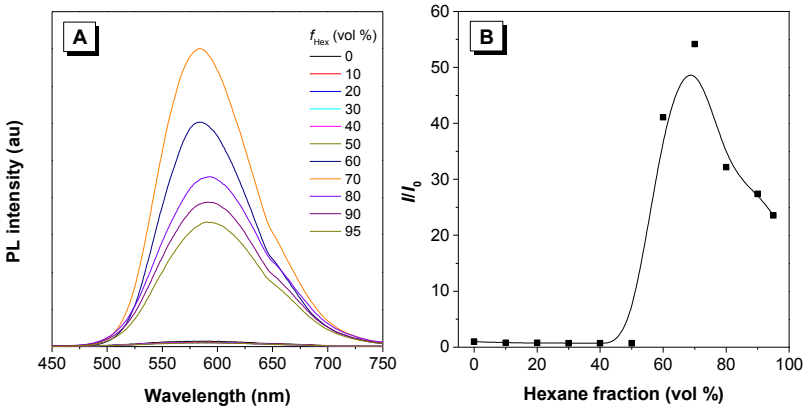

Figure S3. (A) PL spectra of TPE-OP in THF and THF/hexane mixtures with different hexane fractions, [TPE-OP] = 1.0 ×10^{-5} M. Excitation wavelength: 390 nm, ex/em slits = 1.5/1.5 nm. (B) Plot of relative PL intensity of I/I_0 of TPE-OP at 595 nm versus the composition of THF/hexane mixture (f_{Hex}). I_0 = PL intensity of TPE–OP in THF solution. I = PL intensity of TPE-OP in various THF/hexane mixture.

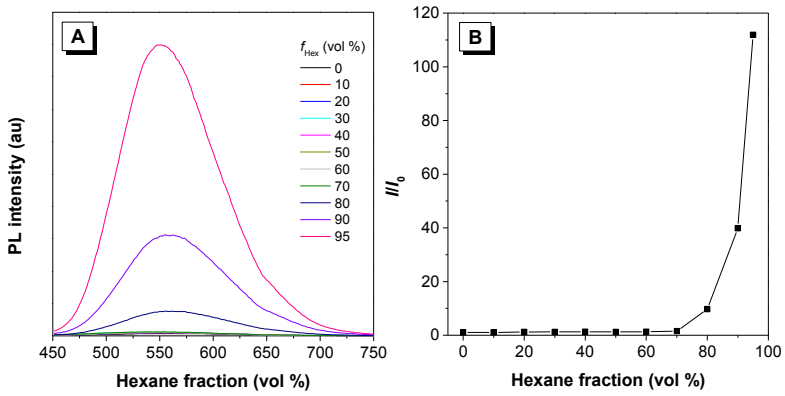

Figure S4. (A) PL spectra of TPE-H in THF and THF/hexane mixture with different hexane fraction, [TPE-H] = 1.0 ×10^{-5} M. Excitation wavelength: 375 nm, ex/em slits = 3/3 nm. (B) Plot of relative PL intensity of I/I_0 of TPE-H at 555 nm versus the composition of THF/hexane mixture (f_{Hex}). I_0 = PL intensity of TPE–H in THF solution. I = PL intensity of TPE-H in various THF/hexane mixture.

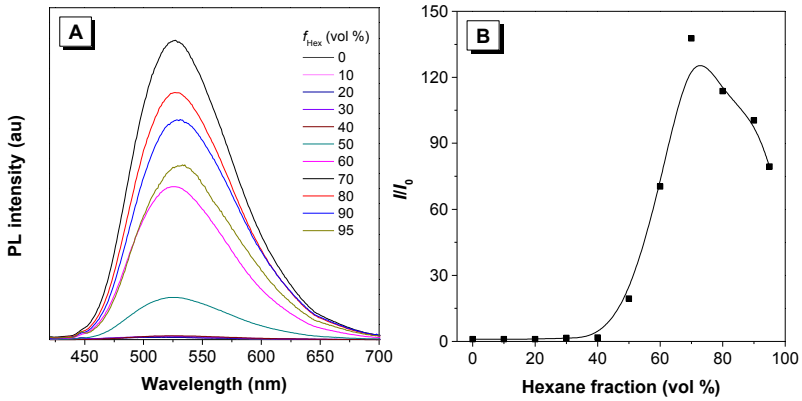

Figure S5. (A) PL spectra of TPE-NO in THF and THF/hexane mixture with different hexane fraction, [TPE-NO] = 1.0 ×10^{-5} M. Excitation wavelength: 350 nm, ex/em slits = 3/3 nm. (B) Plot of relative PL

intensity of I/I_0 of TPE-NO at 525 nm versus the composition of THF/hexane mixture (f_{Hex}). I_0 = PL intensity of TPE–NO in THF solution. I = PL intensity of TPE-NO in various THF/hexane mixture.

4. Mechanochromic luminescence of AIEgens under anisotropic grinding

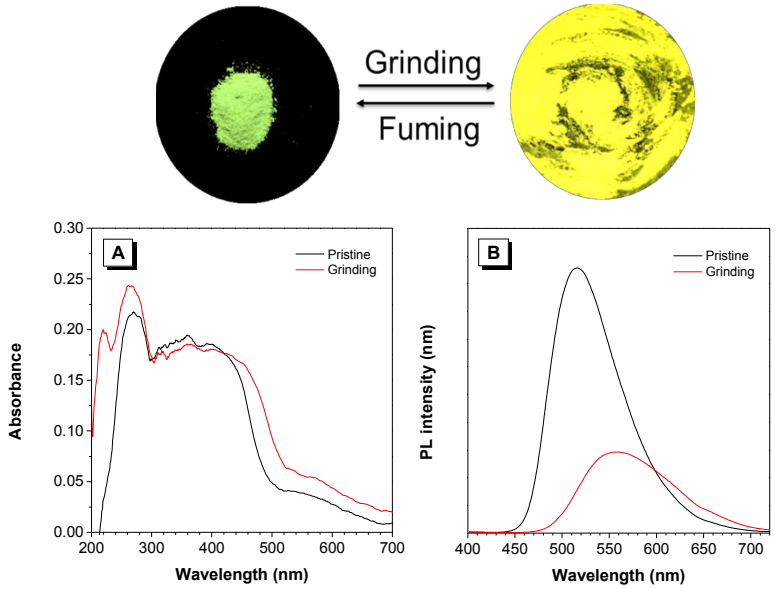

Figure S6. Fluorescent images of reversible mechanochromic luminescence of TPE-H taken under 365 nm UV irradiation. UV-vis (A) and PL spectra (B) of TPE-H before and after grinding. Excitation wavelength: 390 nm, ex/em slits = 3/3 nm.

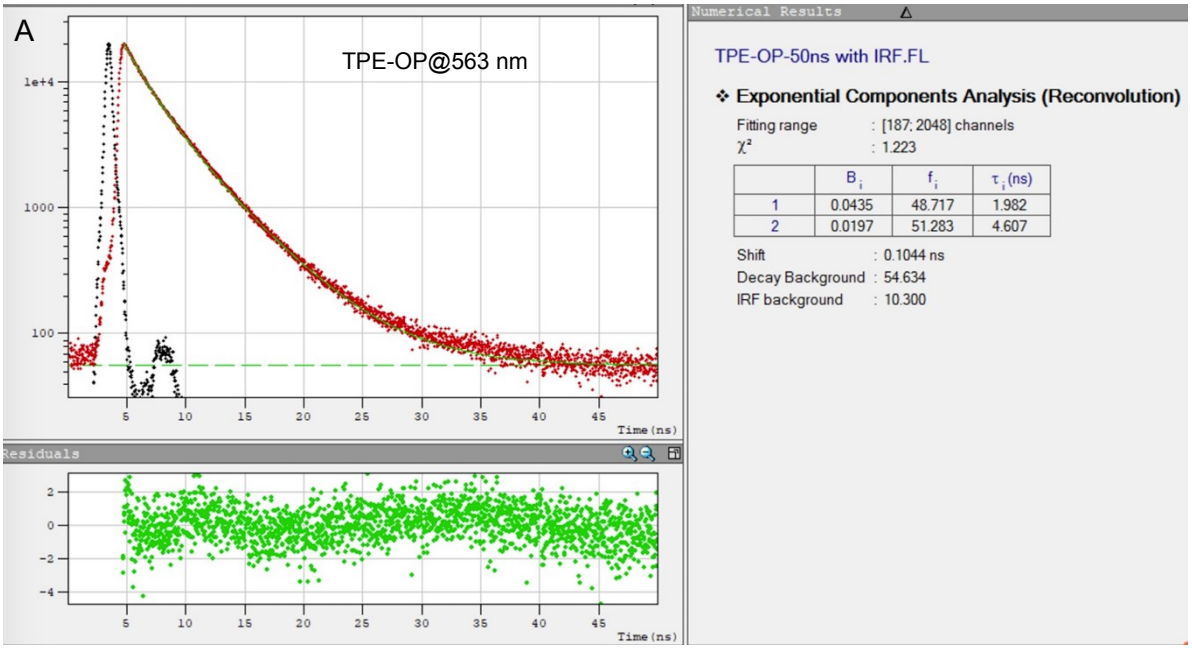

	B_i	f_i	τ_i (ns)
1	0.0435	48.717	1.982
2	0.0197	51.283	4.607

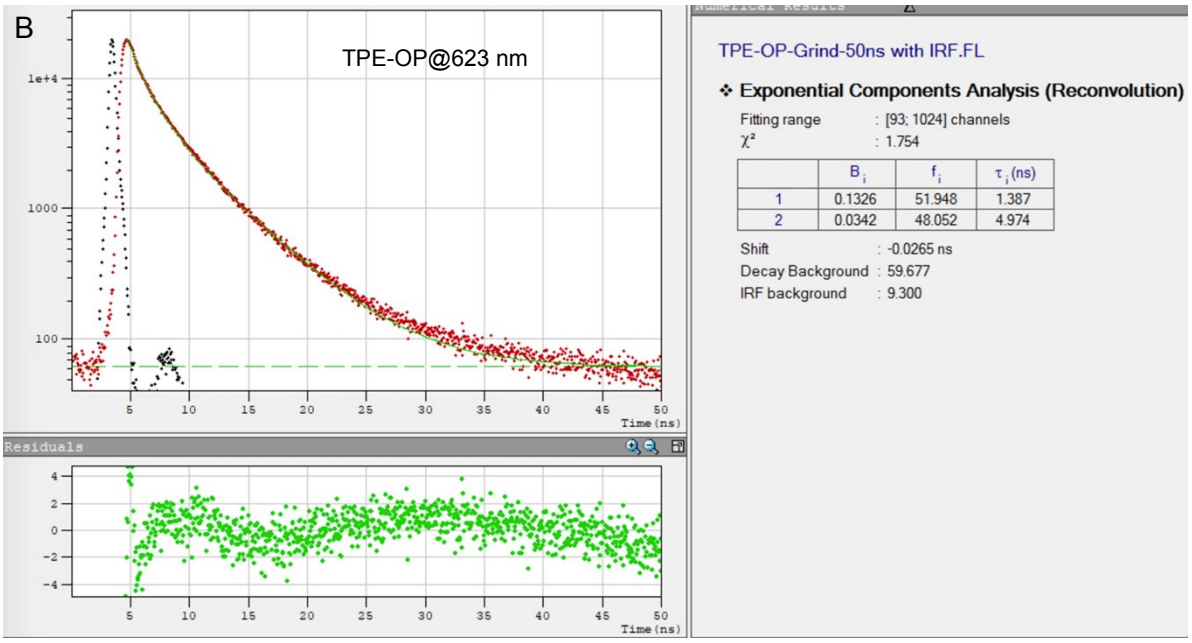

Figure S7. Time-resolved fluorescence decay curves of TPE-OP before (A) and after (B) grinding excited at 375 nm at 300K. A picosecond pulsed diode laser (EPL-375) was used as the light source. The impulse response function (IRF) (black) was from the output of pulsed diode laser.

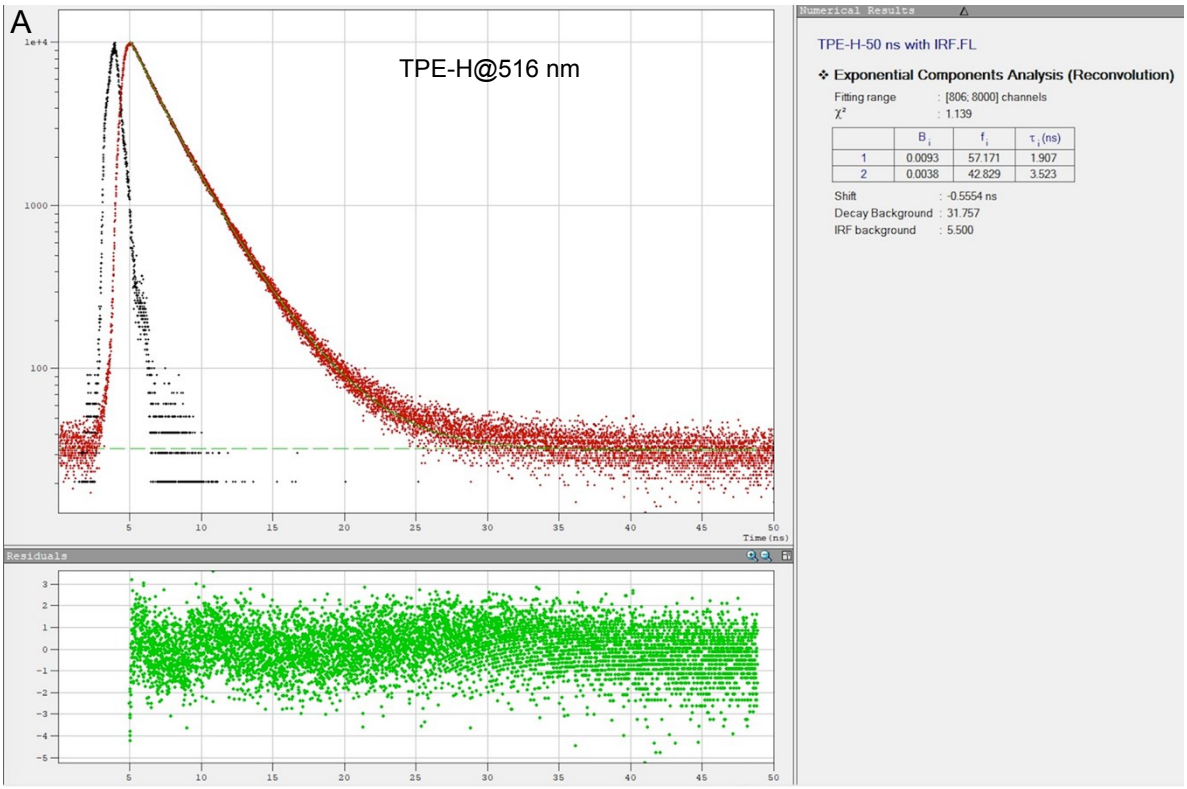

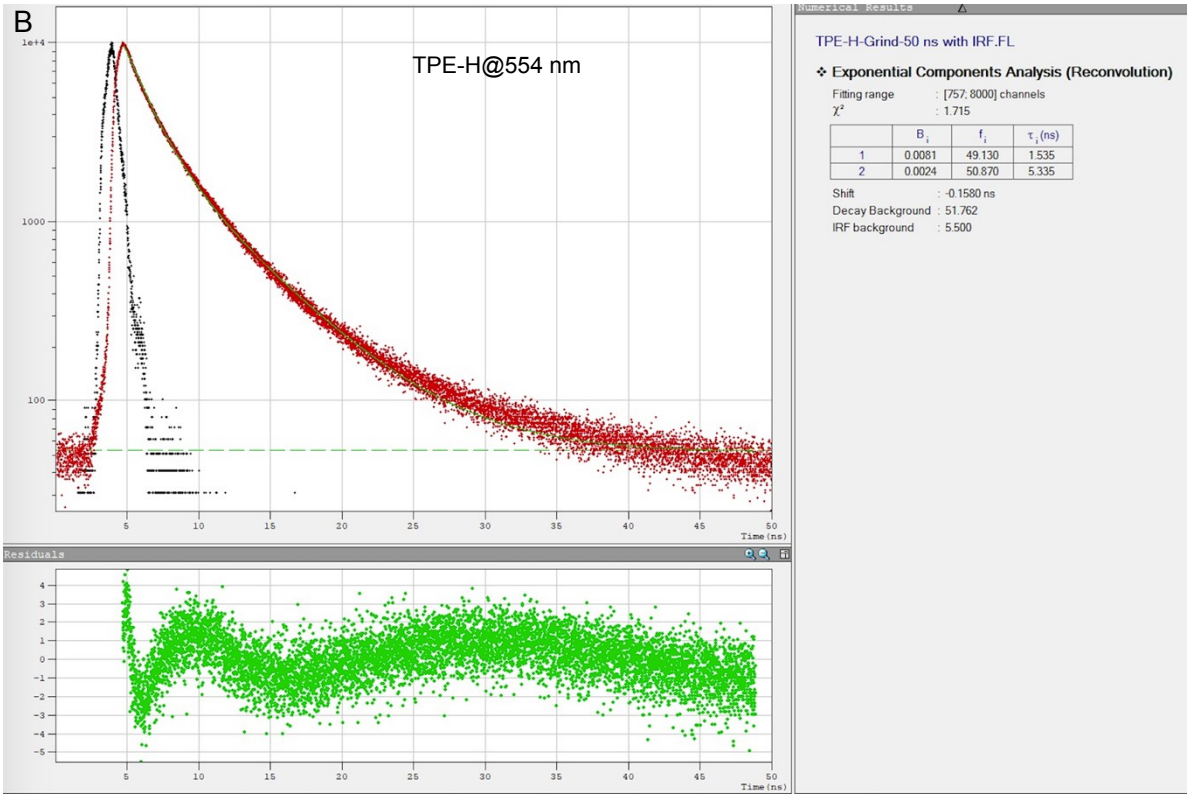

Figure S8. Time-resolved fluorescence decay curves of TPE-H before (A) and after (B) grinding excited at 375 nm at 300K. A picosecond pulsed diode laser (EPL-375) was used as the light source. The impulse response function (IRF) (black) was from the output of pulsed diode laser.

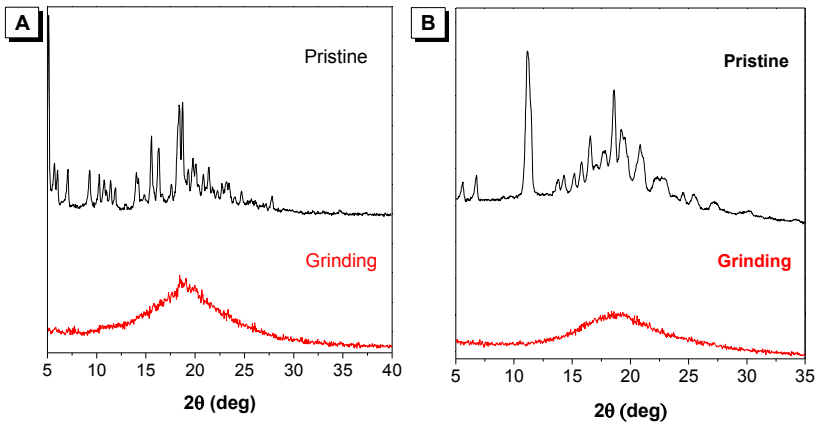

Figure S9. PXRD patterns of pristine and ground powders of TPE-H (A) and TPE-NO (B).

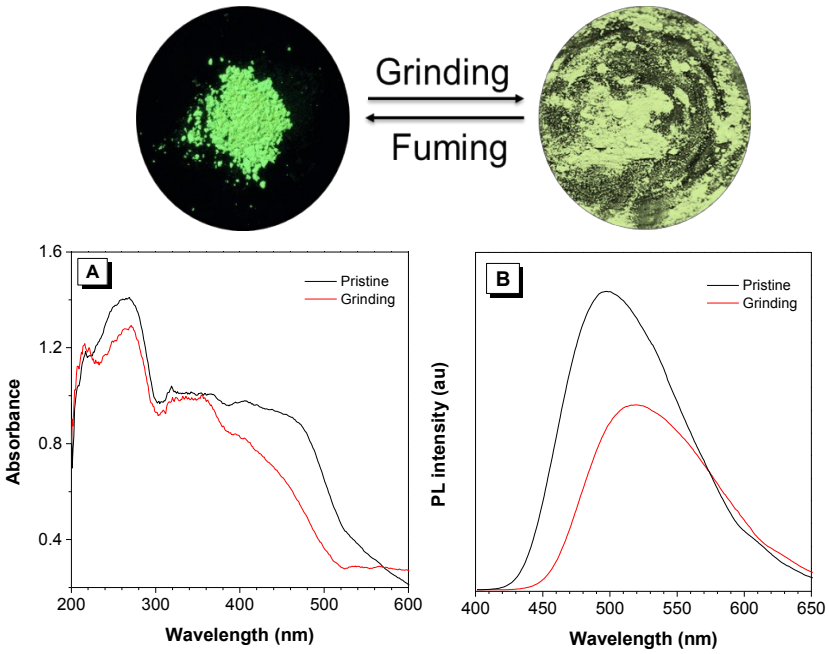

Figure S10. Fluorescent images of mechanochromic luminescence of TPE-NO taken under 365 nm UV irradiation. UV-vis (A) and PL spectra (B) of TPE-NO before and after grinding. Excitation wavelength: 375 nm, ex/em slits = 3/3 nm.

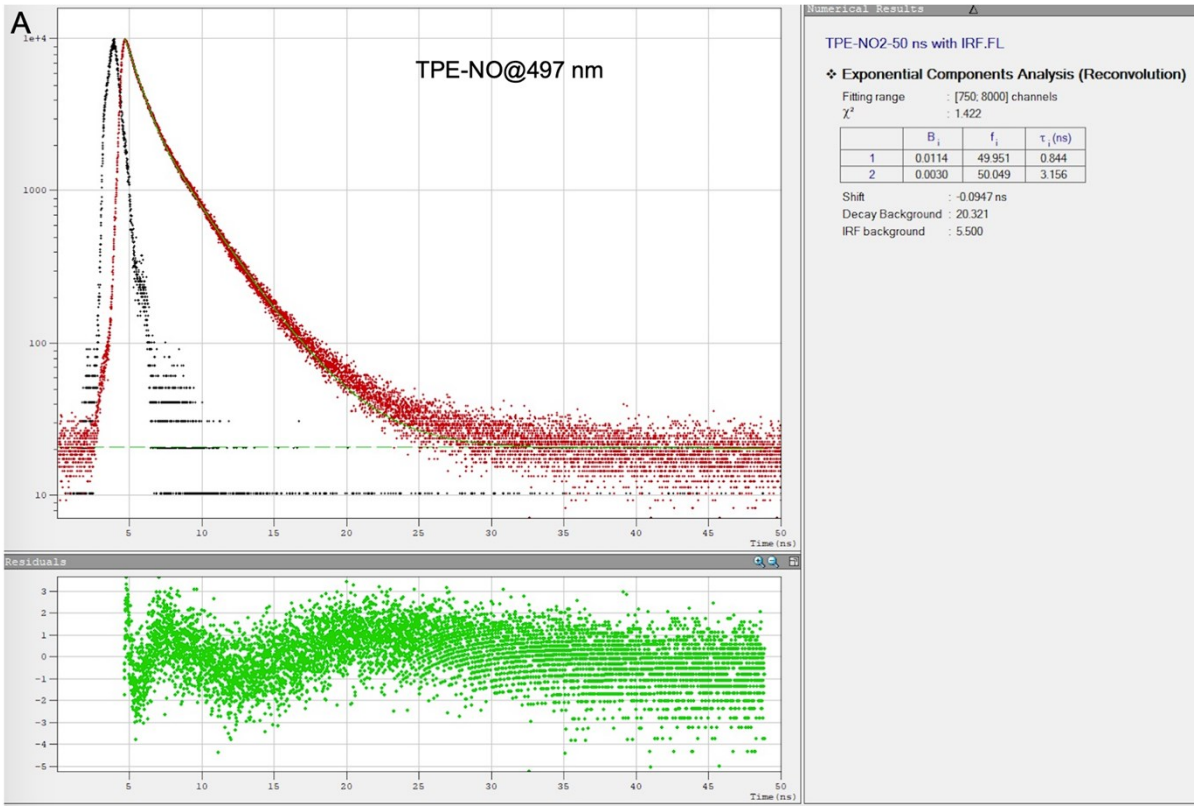

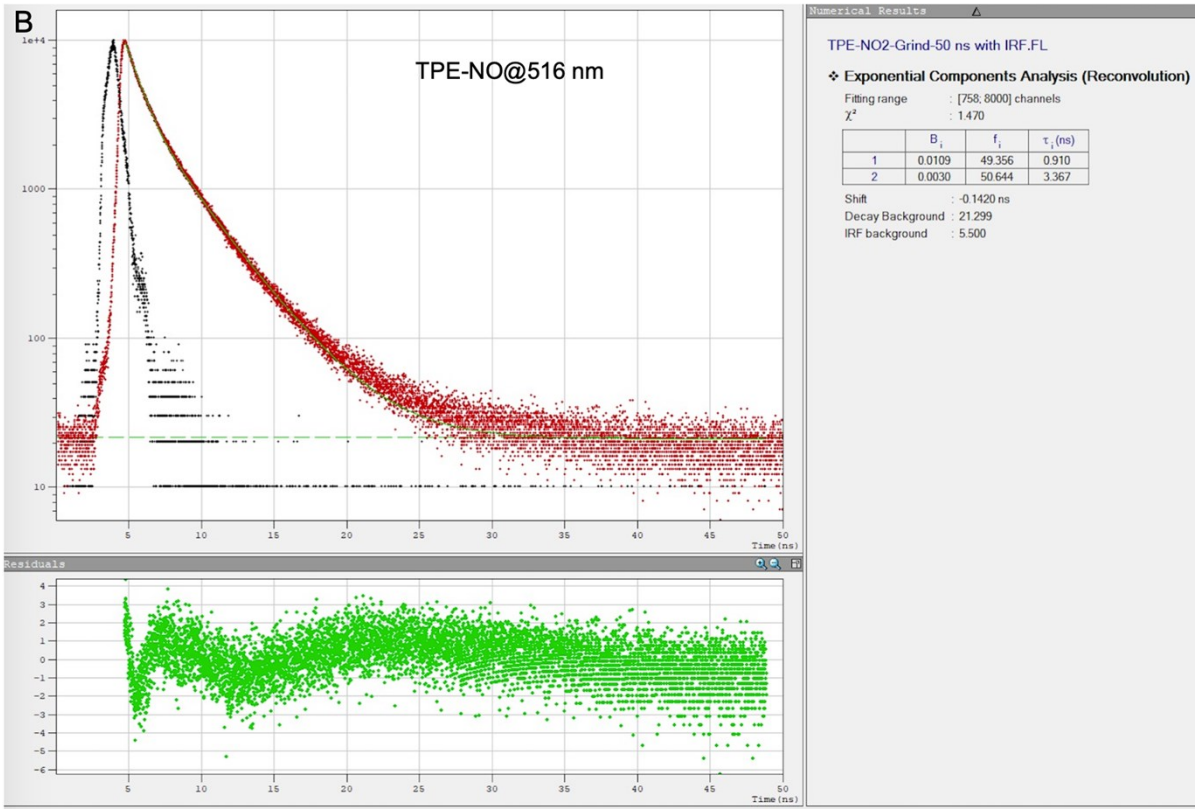

Figure S11. Time-resolved fluorescence decay curves of TPE-NO before (A) and after (B) grinding excited at 375 nm at 300K. A picosecond pulsed diode laser (EPL-375) was used as the light source. The impulse response function (IRF) (black) was from the output of pulsed diode laser.

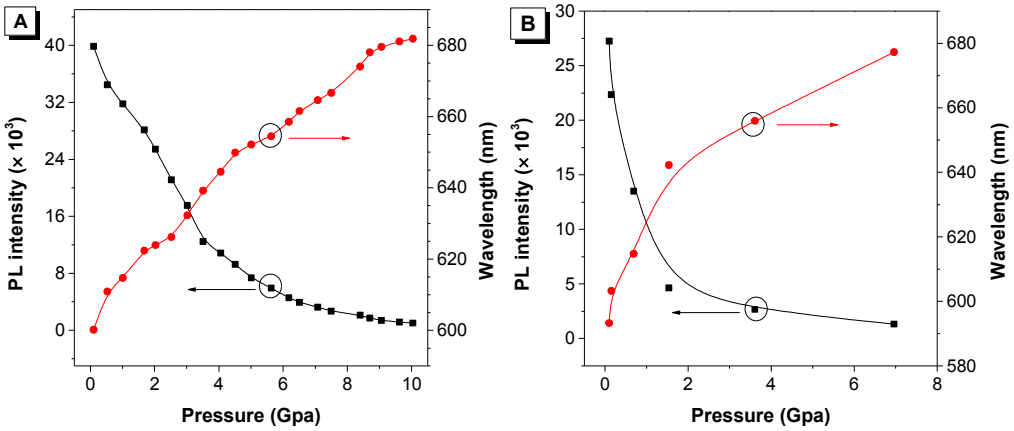

Figure S12. Changes of PL intensity and wavelength of TPE-OP with increasing pressure (A) and decreasing pressure (B).

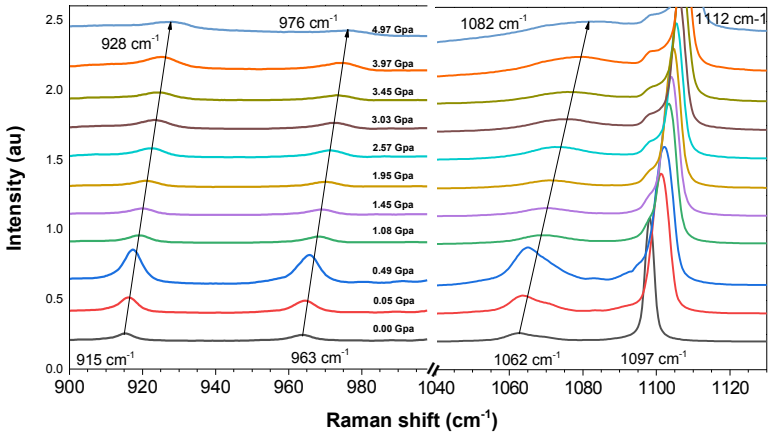

Figure S13. Amplified Raman spectra of TPE-OP.

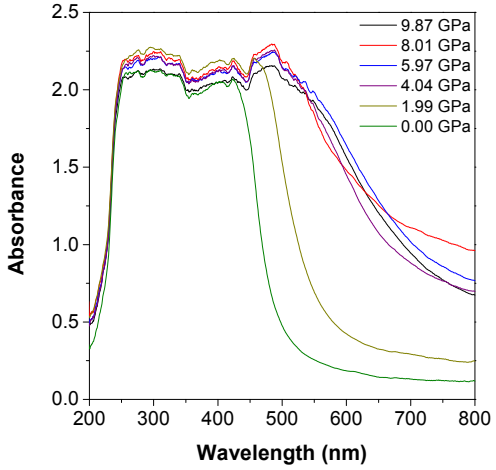

Figure S14. *In-situ* UV-Vis spectra of TPE-H crystal measured during releasing pressure from 9.87 GPa to 1 atm.

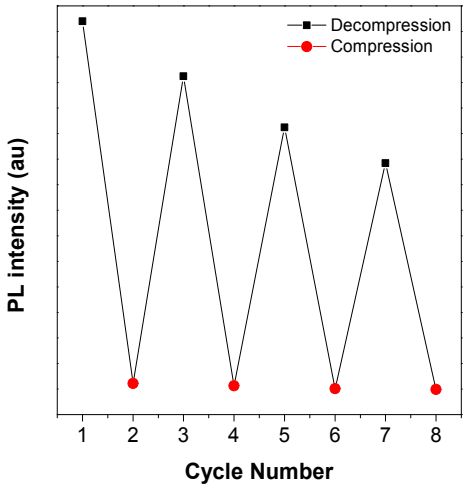

Figure S15. PL intensity change of TPE-H upon repeat increasing pressure and releasing pressure between 1 atm and 10.00 GPa.

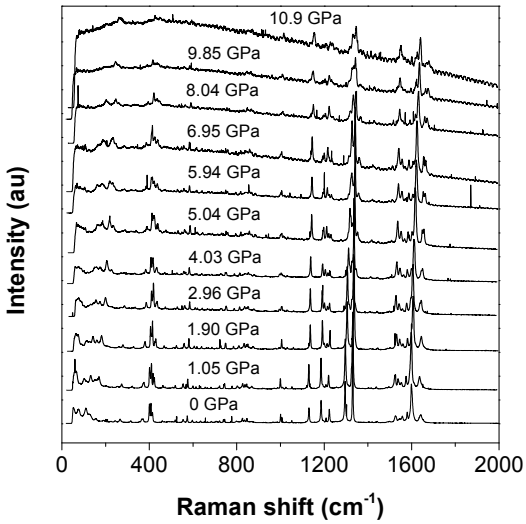

Figure S16. *In-situ* Raman spectra of TPE-H crystal with increasing pressure from 1 atm to 10.9 GPa.

5. Crystal structures of 1A, 1B and 1C.

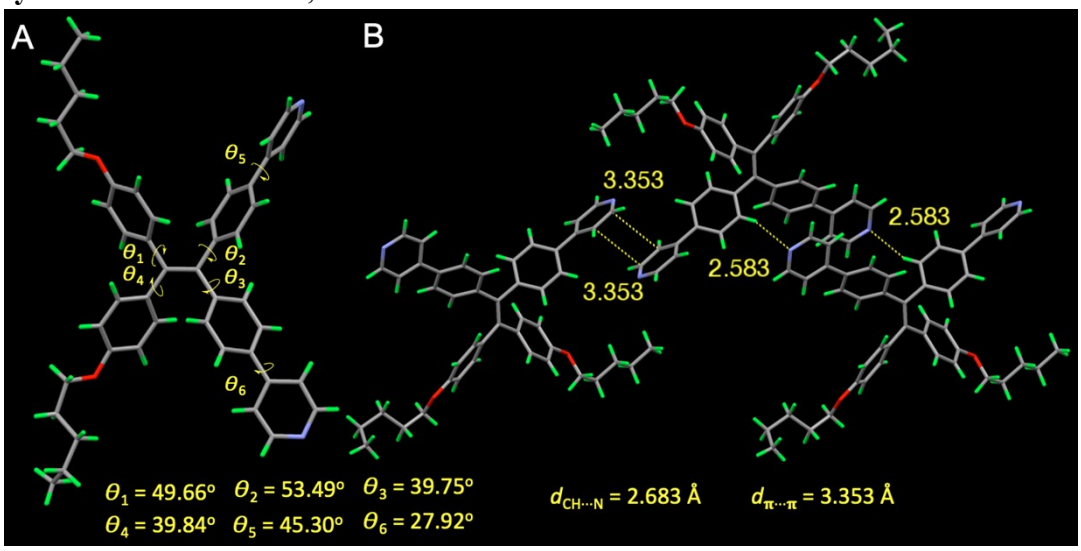

Figure S17. (A) The molecular geometry of **1A** and (B) interactions between adjacent molecules in the crystals. Green: Hydrogen, Grey: Carbon, Red: Oxygen and purple: Nitrogen.

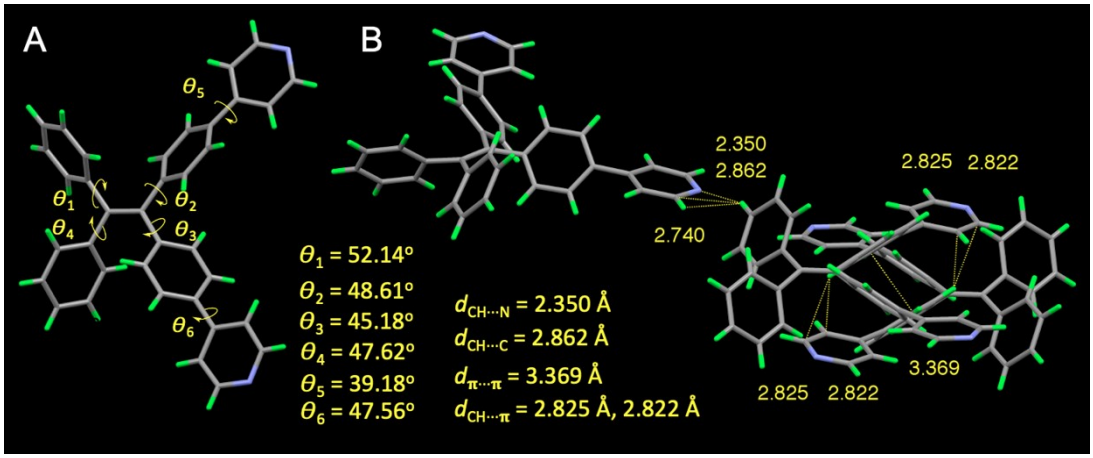

Figure S18. (A) The molecular geometry of **1B** and (B) interactions between adjacent molecules in the crystals. Green: Hydrogen, Grey: Carbon and purple: Nitrogen.

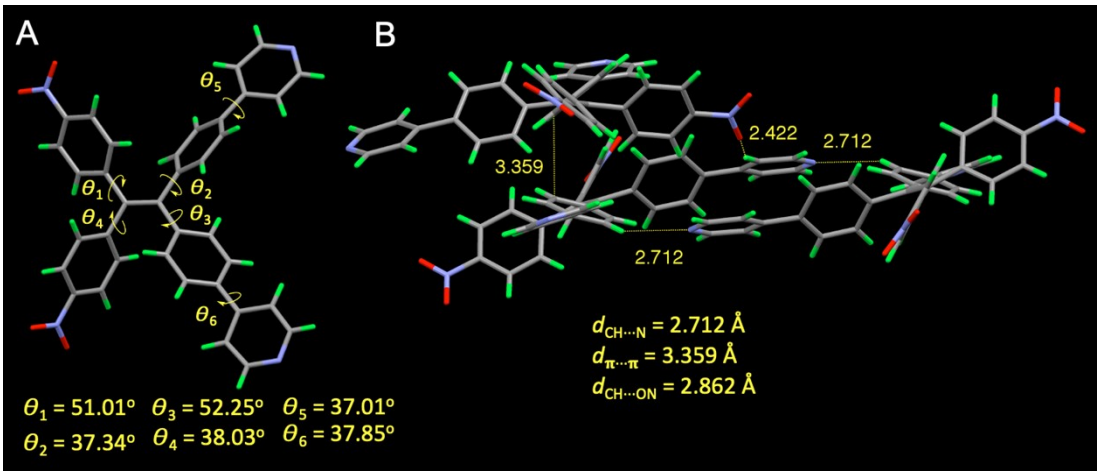

Figure S19. (A) The molecular geometry of **1C** and (B) interactions between adjacent molecules in the crystals. Green: Hydrogen, Grey: Carbon, Red: Oxygen and purple: Nitrogen.

6. Vertical Excitation Energy of TPE-OP, TPE-H and TPE-NO

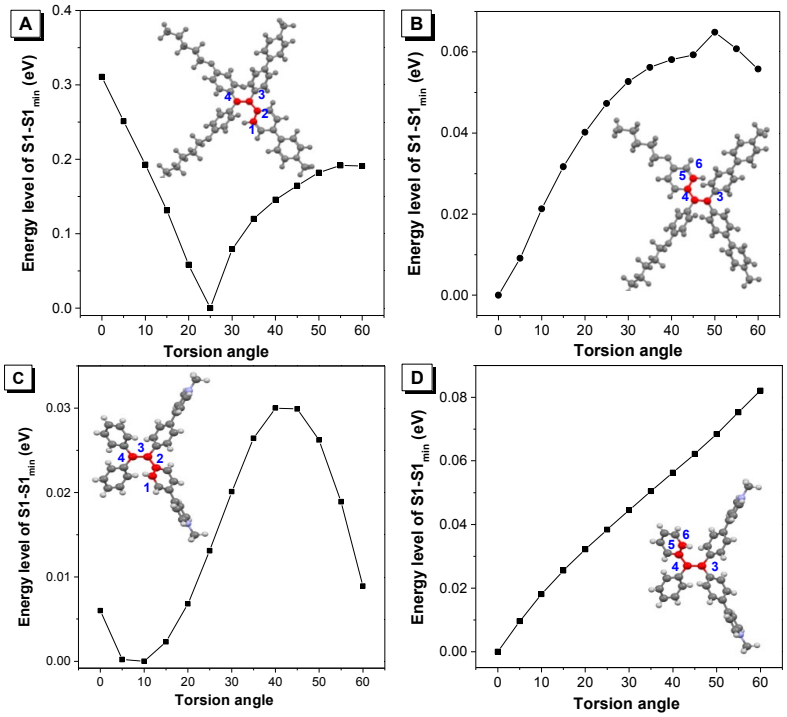

Figure S20. Plot of vertical excitation energy as a function of the chosen torsion angle (highlight in red) during the flipping of different phenyl rings in TPE-OP (A and B) and TPE-H (C and D).

7. Characteristic Spectra of TPE-OP, TPE-H and TPE-NO.

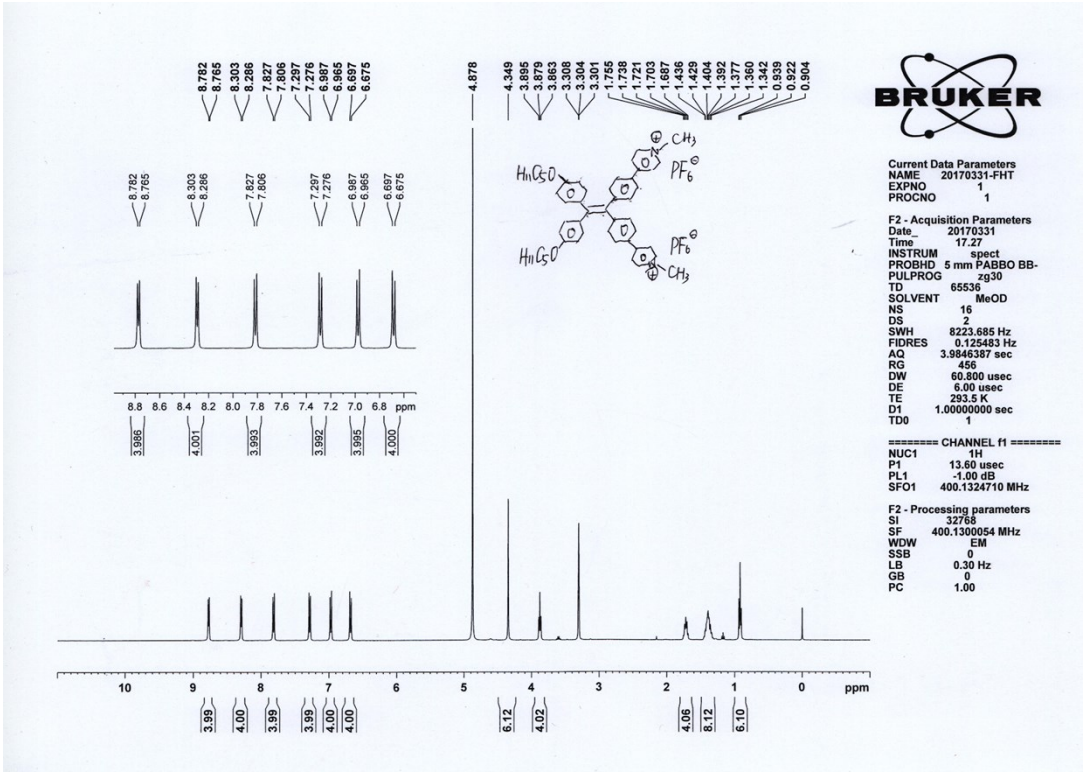

Figure S21. ^{1}H NMR spectrum of TPE-OP in MeOD.

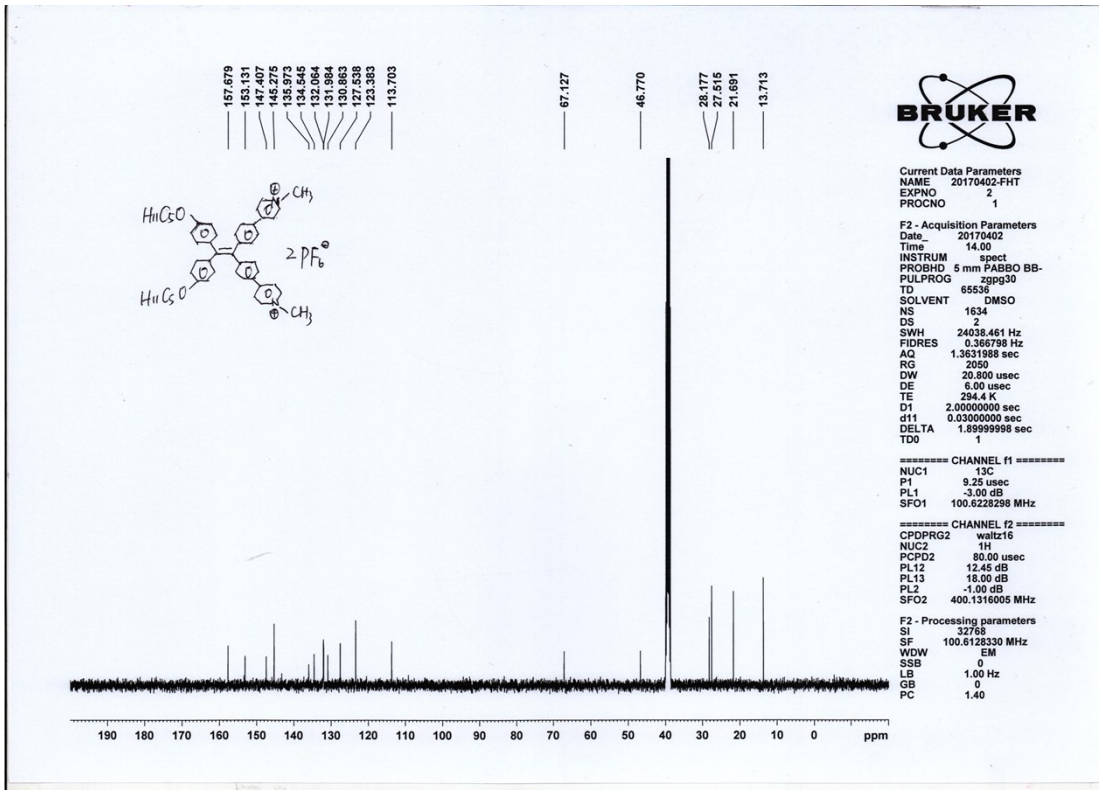

Figure S22. ^{13}C NMR spectrum of TPE-OP in DMSO-d_6.

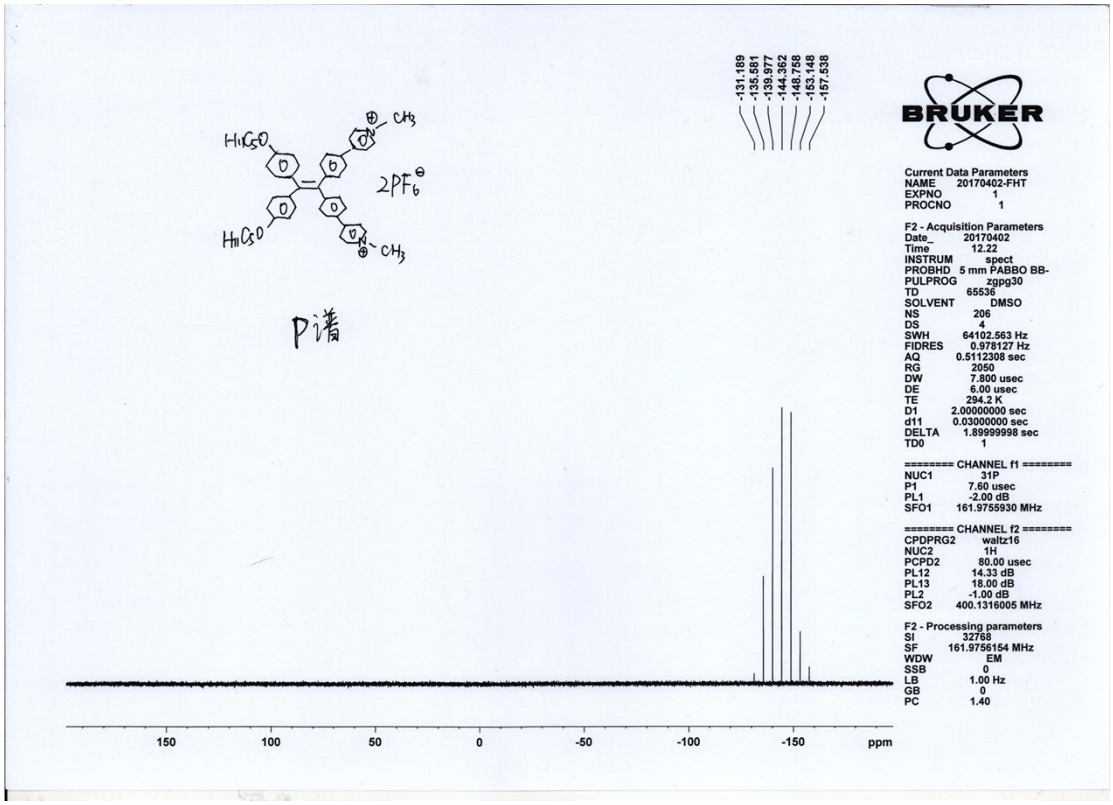

Figure S23. ^{31}P NMR spectrum of TPE-OP in DMSO-d_6.

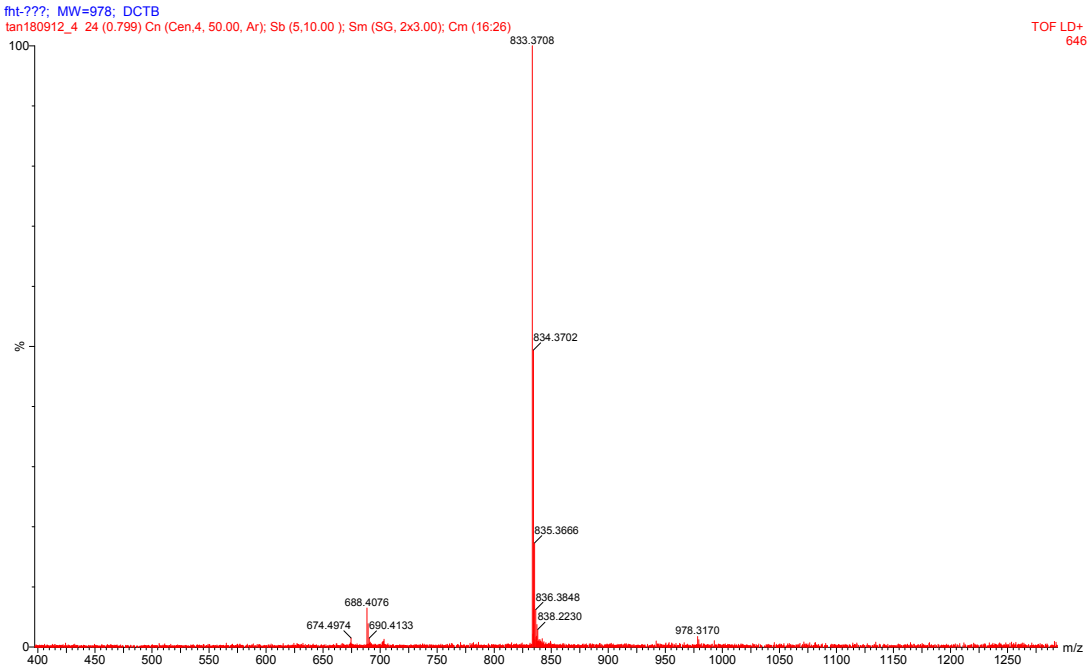

Figure S24. HRMS spectrum of TPE-OP.

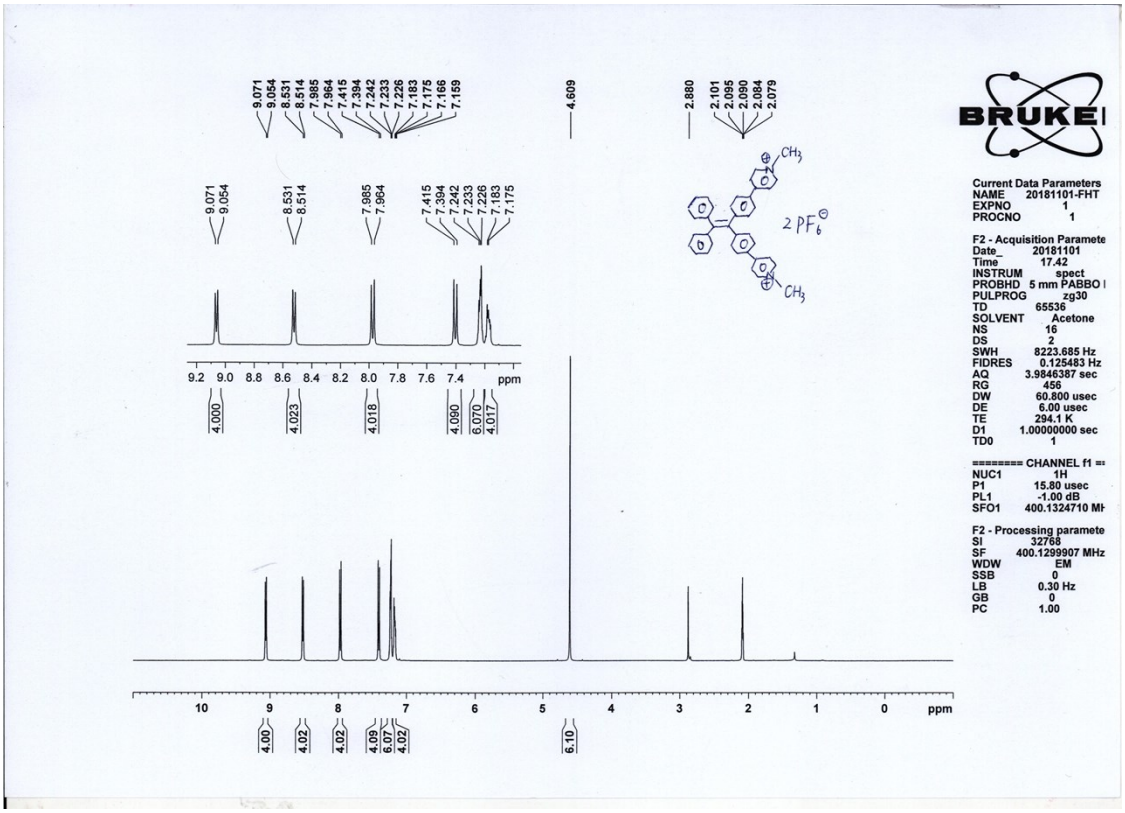

Figure S25. ^{1}H NMR spectrum of TPE-H in Acetone-d_6.

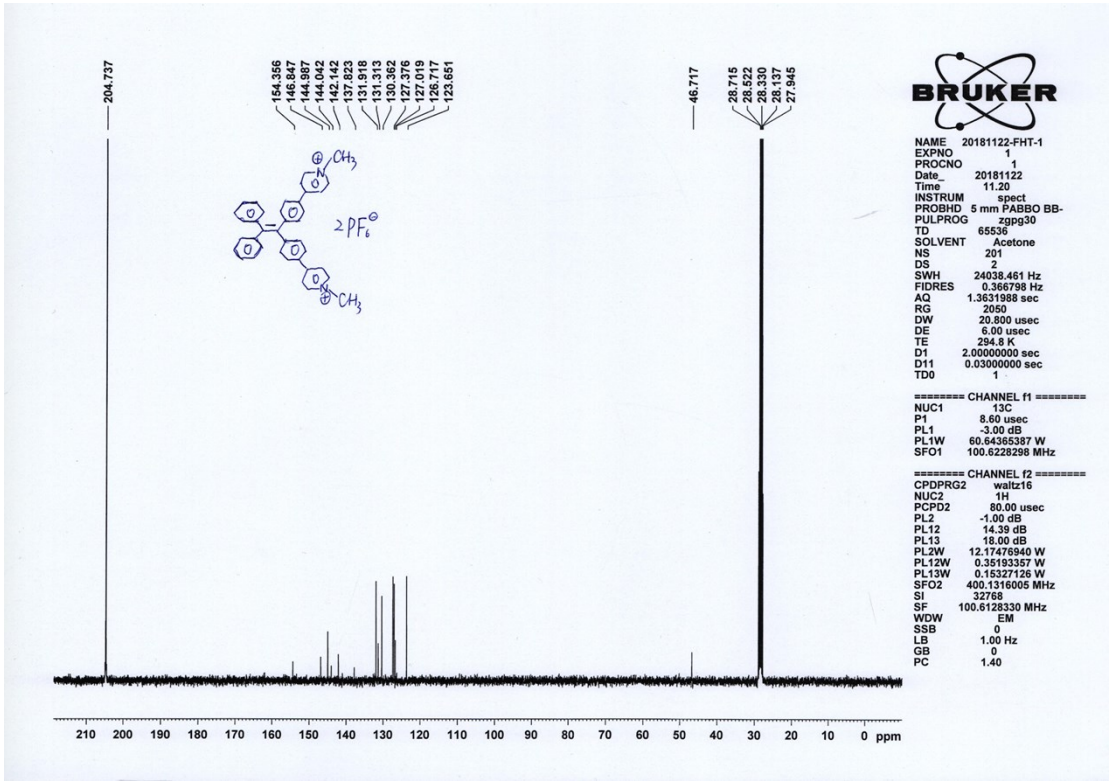

Figure S26. ^{13}C NMR spectrum of TPE-H in Acetone-d_6.

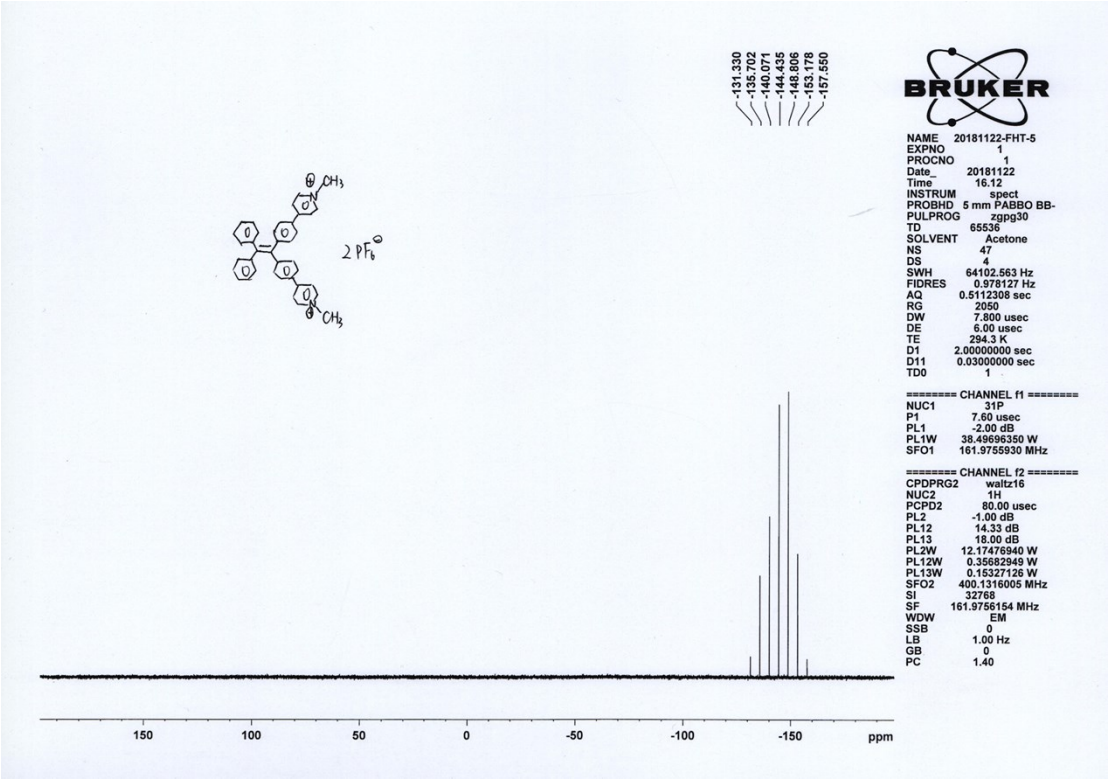

Figure S27. ^{31}P NMR spectrum of TPE-H in Acetone-d_6.

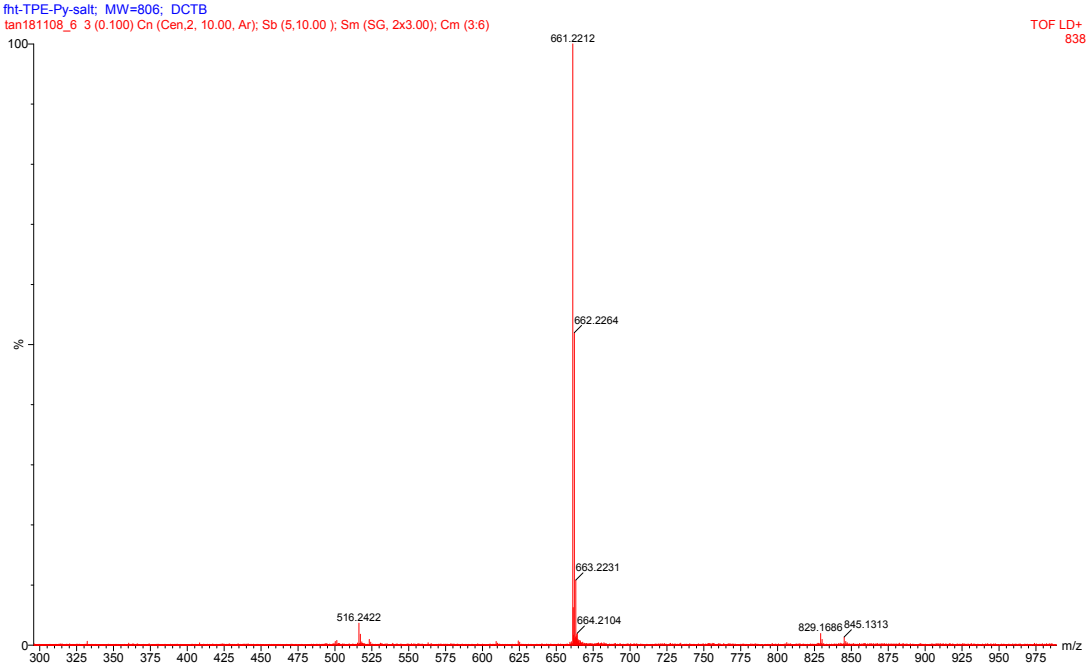

Figure S28. HRMS spectrum of TPE-H.

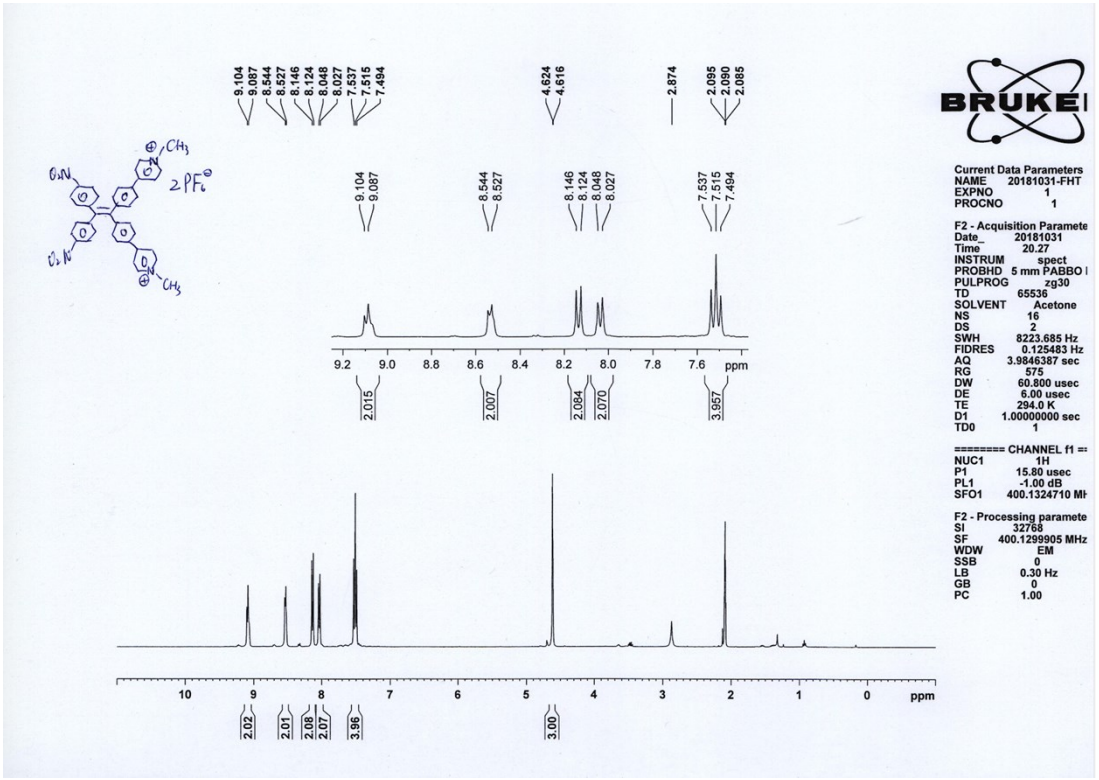

Figure S29. ^{1}H NMR spectrum of TPE-NO in Acetone-d_6.

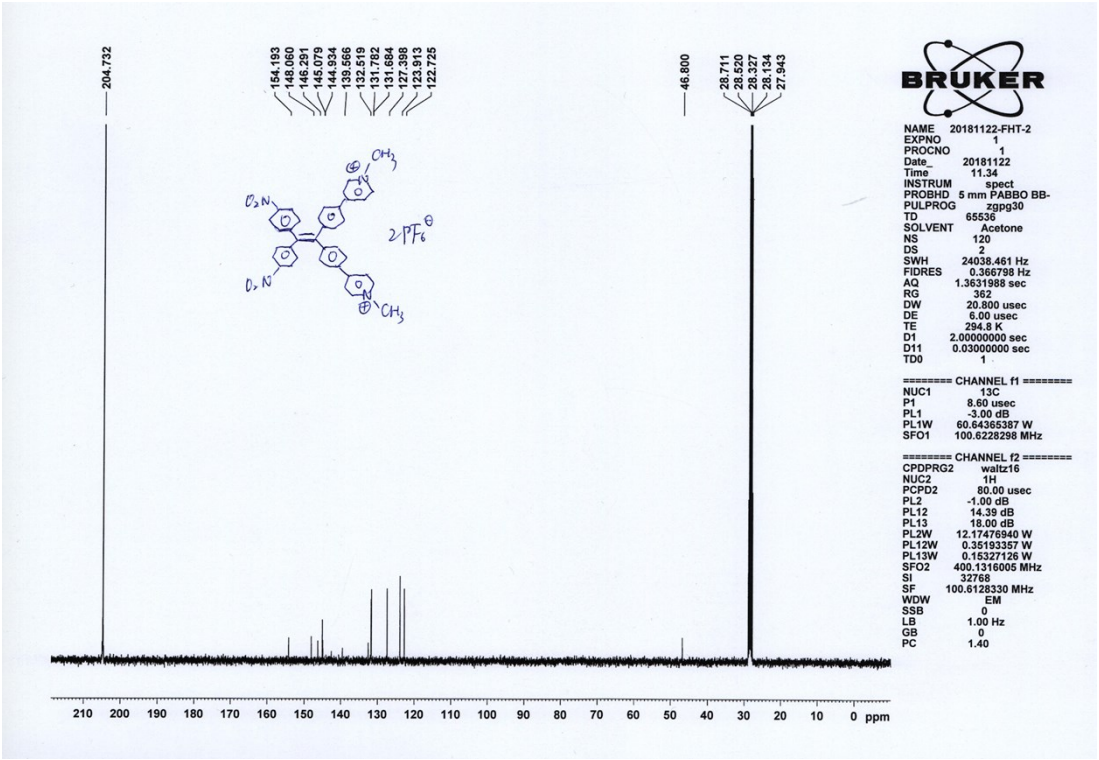

Figure S30. ^{13}C NMR spectrum of TPE-NO in Acetone-d_6.

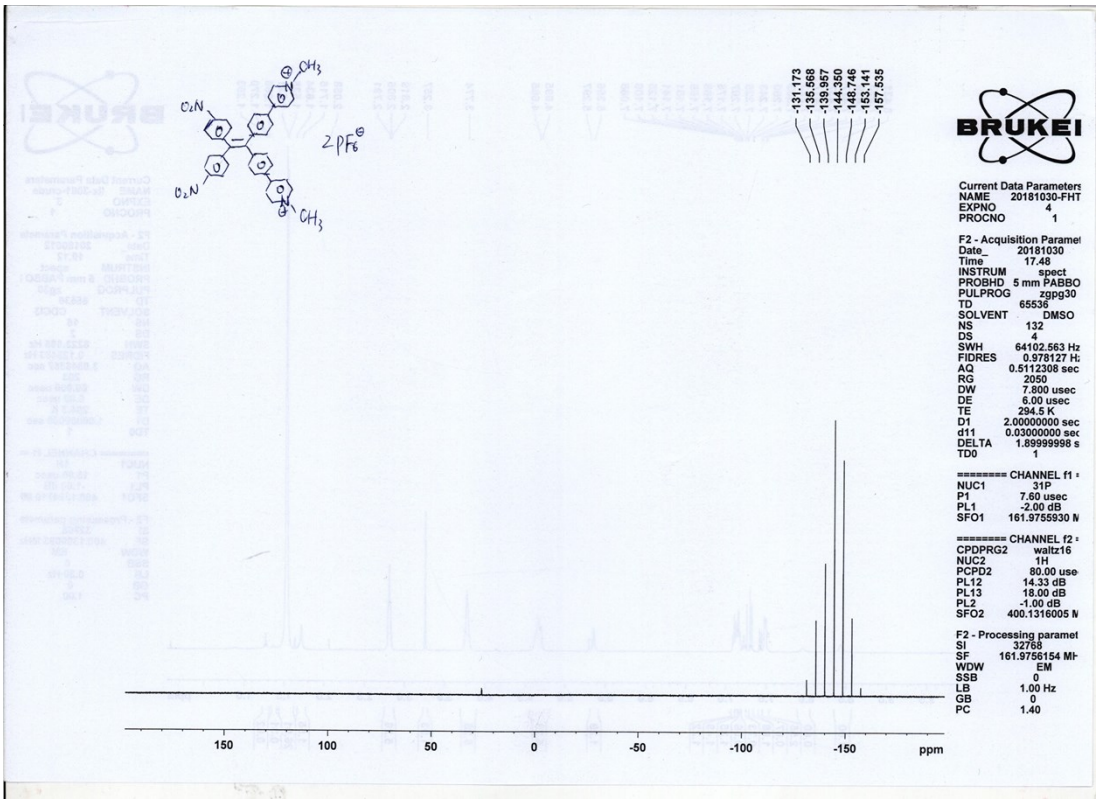

Figure S31. ^{31}P NMR spectrum of TPE-NO in DMSO-d_6

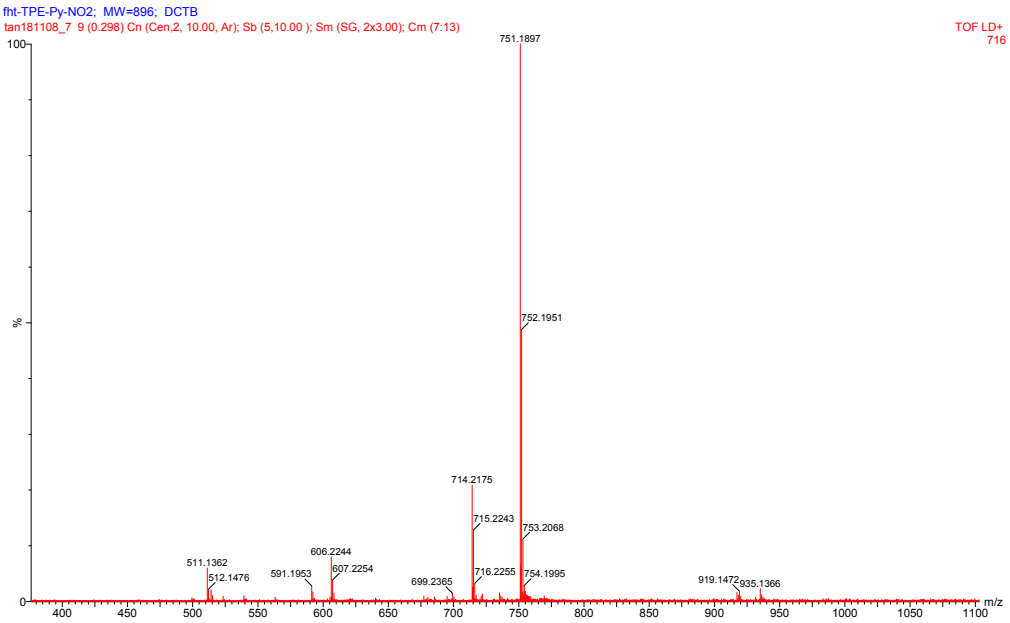

Figure S32. HRMS spectrum of TPE-NO.

8. Reference:

[1] H.-T. Feng, J.-B. Xiong, J. Luo, W.-F. Feng, D. Yang, Y.-S. Zheng, *Chem. Eur. J.* **2017**, *23*, 644 – 651

[2] X. Yan, H. Wang, C. E. Hauke, T. R. Cook, M. Wang, M. L. Saha, Z. Zhou, M. Zhang, X. Li, F. Huang, P. J. Stang, *J. Am. Chem. Soc.* **2015**, *137*, 48, 15276-15286.

[3] H.-T. Feng, S. Zou, M. Chen, F. Xiong, M.-H. Lee, L. Fang, B. Z. Tang, *J. Am. Chem. Soc.* **2020**, *142*, 11442−11450.